Available online at www.sciencedirect.com
ScienceDirect
Journal of Structural Biology 160 (2007) 275–286
Journal of Structural Biology
www.elsevier.com/locate/yjsbi

The role of lipids and salts in two-dimensional crystallization of the glycine–betaine transporter BetP from *Corynebacterium glutamicum*

Ching-Ju Tsai [a], Christer S. Ejsing [b], Andrej Shevchenko [b], Christine Ziegler [a,*]

[a] *Max Planck Institute of Biophysics, Department of Structural Biology, Max-von-Laue Strasse 3, 60438 Frankfurt, Germany*
[b] *Max Planck Institute of Molecular Cell Biology and Genetics, 01307 Dresden, Germany*

Received 1 May 2007; received in revised form 6 September 2007; accepted 12 September 2007
Available online 19 September 2007

Abstract

The osmoregulated and chill-sensitive glycine–betaine transporter (BetP) from *Corynebacterium glutamicum* was reconstituted into lipids to form two-dimensional (2D) crystals. The sensitivity of BetP partly bases on its interaction with lipids. Here we demonstrate that lipids and salts influence crystal morphology and crystallinity of a C-terminally truncated BetP. The salt type and concentration during crystallization determined whether crystals grew in the form of planar-tubes, sheets or vesicles, while the lipid type influenced crystal packing and order. Three different lipid preparations for 2D crystallization were compared. Only the use of lipids extracted from *C. glutamicum* cells led to the formation of large, well-ordered crystalline areas. To understand the lipid-derived influence on crystallinity, lipid extracts from different stages of the crystallization process were analyzed by quantitative multiple-precursor ion scanning mass spectroscopy (MS). Results show that BetP has a preference for fatty acid moieties 16:0–18:1, and that a phosphatidyl glycerol (PG) 16:0–18:1 rich preparation prevents formation of pseudo crystals.

Keywords: Membrane proteins; 2D crystallization; Lipid species; Mass spectroscopy; Multiple-precursor ion scanning; Electron microscopy

1. Introduction

Two-dimensional (2D) and three-dimensional (3D) crystallization are the standard methods to obtain structural information of membrane proteins. Prior to crystallization, membrane proteins have to be extracted from their native environment by amphiphilic detergents. Membrane proteins are crystallized after purification in detergent solution and most 3D crystallization techniques maintain this non-physiological, detergent-rich environment (Hunte et al., 2005; Yildiz et al., 2006). During 2D crystallization, a native like environment is restored by incorporation of the protein into a lipid bilayer. Another advantage of 2D crystals is that the protein does not have crystal contacts in all dimensions and thus conformational changes can be often induced without destroying crystal order (Ruprecht et al., 2004; Vinothkumar et al., 2005). Single-layered 2D crystals are classified into three morphologies: sheets, planar-tubes, and vesicles (Mosser, 2001). The morphology of small vesicle is frequently obtained at the initial screening stage of 2D crystallization and indicates successful protein reconstitution. Sheet-like and planar-tubular crystals form less readily but tend to have a higher degree of order and are usually favored for data collection. In the case of the bacterial oxalate transporter OxlT, the crystal morphology of sheets and planar-tubes can be controlled by varying the salt concentrations and temperatures during crystallization (Heymann et al., 2003). Apart from crystal morphology, crystal qualities are judged by several aspects: size of the crystalline area, diffraction intensity, reflection sharpness and resolution. Lipid-to-protein ratio (LPR) is the most important factor in influencing crystal quality (Schmidt-Krey et al., 1998, 2007). If the LPR is chosen too high, proteins are only loosely packed. Is it too low,

* Corresponding author. Fax: +49 69 6303 2209.
E-mail address: Christine.Ziegler@mpibp-frankfurt.mpg.de (C. Ziegler).

1047-8477/$ - see front matter © 2007 Elsevier Inc. All rights reserved.
doi:10.1016/j.jsb.2007.09.008

most of the proteins can not be incorporated and aggregate (Schmidt-Krey et al., 1998; Zhuang et al., 1999). Beside the amount, the type of lipid is crucial for successful 2D crystallization of a protein. Typically membrane protein preparations contain co-purified lipids from their native tissue or the expression organism. Additional lipids are usually added to facilitate 2D crystallization, such as synthetic lipids and natural lipids extracted from homologous or heterologous organisms.

Specific lipids can not only stabilize membrane proteins but also benefit structural integrity, enzymatic activity and stability of oligomeric states (Palsdottir and Hunte, 2004; Standfuss et al., 2005). In the case of the secondary transporter BetP, the positively charged C-terminus acts as an osmosensor which directly interacts with the lipid membrane when there is low osmolarity (Rübenhagen et al., 2000; Schiller et al., 2004, 2006). Accordingly an enrichment of the negatively charged phosphatidyl glycerol (PG) in proteoliposome membranes elevates the osmoactivation threshold and increases osmotic tolerance of BetP (Rübenhagen et al., 2000). Besides being an osmosensor, BetP is also activated by low temperatures. This chill activation is not involving the C-terminus and is only observed when BetP is expressed in *Corynebacterium glutamicum* cells but not in *Escherichia coli* cells, possibly due to differences in the lipid content of the cell membranes (Özcan et al., 2005).

The *C. glutamicum* plasma membrane comprises three main glycerophospholipid classes: PG, cardiolipin (CL) and phosphatidyl inositol (PI), having predominantly palmitic acid (16:1) and oleic acid (18:1) moieties (Hoischen and Krämer, 1990). As the membrane environment is relevant to both osmo- and chill-activation mechanisms of BetP, it is likely to encounter a lipid-derived effect on crystallization of BetP. In this report we crystallize a C-terminally truncated BetP mutant with different lipid preparations and quantify the lipids before and after crystallogenesis by a powerful high-throughput oriented mass spectroscopic tool designed for comprehensive and quantitative analysis of molecular lipid species (Ejsing et al., 2006). Results show how the different lipids influence size and order of the crystals and how crystal morphology can be controlled by changing salinity during crystallization.

2. Materials and methods

2.1. Protein expression and purification

The plasmid pASK-IBA5*betPΔC45* containing an N-terminal StrepII-tag was constructed as described (Schiller et al., 2004), and transformed into *E. coli* C43 cells (Dumon-Seignovert et al., 2004). Protein overexpression and membrane isolation were essentially as described (Ziegler et al., 2004). Strep-BetPΔC45 was extracted with dodecyl maltoside (DDM) that was added stepwise until a final concentration to 1.5% (w/v) was reached. After stirring on ice for 30 min, the solubilizate was centrifuged for 45 min at 140,000*g*. The supernatant fraction containing solubilized Strep-BetPΔC45 was purified by Strep-tag/StrepTactin affinity chromatography (IBA GmbH) using a 4-ml column of StrepTactin resin. The column was pre-equilibrated with buffer Na^+ (50 mM, pH 7.5, Tris–HCl, 200 mM NaCl, 10% glycerol). The supernatant was diluted with two volumes of buffer Na^+ before addition to the column to allow binding of proteins to StrepTactin. The column was washed with six bed volumes of buffer Na^+ containing 0.04% DDM before Strep-BetPΔC45 was eluted with buffer Na^+ containing 0.04% DDM and 5 mM desthiobiotin. The eluate was collected in 0.5–1 ml fractions, and the fractions higher than 3 mg/ml were combined and used for 2D crystallization. All steps of purification were carried out at 4 °C.

2.2. Preparation of C. glutamicum lipid extract

Corynebacterium glutamicum strain Cgl*ΔotsAΔtreSΔϖtreY* was cultivated in minimal medium CGXII (Keilhauer et al., 1993) at 30 °C. Membranes were prepared as described (Ziegler et al., 2004) and homogenized into chloroform/methanol (2:1, v/v) with a dilution factor of 20 of the initial volume of the membrane suspension. The homogenization was carried out at room temperature for 4 h. Aggregates were removed by passing through filter paper (Whatman, No. 4). The filtrate was mixed with 0.88% KCl aqueous solution in quarter volume of the organic phase in the filtrate, vigorously shaken, and settled overnight at 4 °C for phase separation. The lower organic phase was collected and dried in a rotary vacuum evaporator. Dextran gel (0.2 g, Sephadex G-25 medium, Amersham Pharmacia) was added to absorb inorganically soluble contaminants, and washed three times with chloroform. After removal of the dextran gel the total lipid extract was re-dissolved in chloroform. The *C. glutamicum* lipid extract was examined by thin-layer chromatography and subjected to quantitative multiple precursor ion scanning analysis.

2.3. 2D crystallization

CL from bovine heart, *E. coli* polar lipid extract and 1-palmitoyl-2-oleoyl-*sn*-glycerol-3-[phospho-*rac*-(1-glycerol)] (PG 16:0–18:1) were purchased from Avanti Polar Lipids, Inc. (Alabaster, AL). *C. glutamicum* lipid extract was prepared as described above. *E. coli* polar lipid extract and bovine CL were mixed to 3:2 (w/w). Chloroform-dissolved lipids were dried by evaporation and solubilized into 1% decyl maltoside (DM, Glycon) at a final concentration of 4 mg/ml. Protein–lipid–detergent mixtures were adjusted to contain 2.0–2.5 mg/ml protein, 0.15% DM, and an LPR of 0.1–0.2 (w/w). The co-purified *E. coli* lipids in protein samples were not considered in the LPR. Following incubation at room temperature for 30 min, detergent was removed by dialysis in Mini-Slide-A-lyzers (Pierce, Rockford, IL) having a molecular weight cutoff of 10 kDa against 0.2–1 L of 50 mM Tris–HCl, pH 7.5, 5% glycerol, 5% 2-methyl-2,4-pentanediol (MPD), 3 mM

NaN_3, 50–600 mM monovalent salt (KCl, NaCl, or LiCl), and 4 mM $CaCl_2$. The dialysis was carried out at 37 °C using *E. coli* polar lipid extract/CL (3:2), at 30 °C using *C. glutamicum* lipid extract, and at 30 °C for the crystallization with synthetic PG 16:0–18:1. The final sample volume after three weeks of dialysis was expanded to 80–150 μl, corresponding to 0.8–1.6 mg protein/ml.

2.4. Data collection and image processing

2D crystals were negatively stained with 1% uranyl acetate on a carbon-coated copper grid and screened for crystalline areas by imaging on films in an FEI CM120 electron microscope. Frozen-hydrated specimens for data collection were prepared by the back-injection method using 10% glucose to float a $4 \times 4\ mm^2$ carbon film (Wang and Kühlbrandt, 1991; Williams et al., 1999), and transferred into a JEOL 3000SFF electron microscope equipped with a super-fluid helium stage and a field emission gun. Images were taken on Kodak SO-163 electron emulsion films at a magnification of 45,000 or 53,000 with an exposure procedure of spot scanning, corresponding to a total electron dose of 10–20 electron/$Å^2$. Areas of 6000×6000 pixels were selected by optical diffraction and digitized by a Zeiss SCAI scanner with a scanning pixel size of 7 μm. Scanned areas were corrected for lattice disorder and the contrast transfer function by using the MRC image processing package (Crowther et al., 1996). A Fourier transform of the digitized image was calculated (FFTRANS) and displayed by Ximdisp (Smith, 1999). The unit cell parameters were determined by manually selecting the lattice dimensions in the Fourier transform image. Three rounds of unbending were used, with a reference area of 1%, 0.7%, and 0.25% of the total pixel area for the unbendings one after another (CCUNBENDK). The position of the reference area was evaluated by the cross-correlation map between the whole image and the chosen reference area (QUADSERCHK). The phase and amplitude were printed out for each reflection (MMBOXA). The defocus and astigmatism values were calculated by CTFFIND2 (Grigorieff, 1998). The determined phases were corrected for the contrast transfer function (CTFAPPLY). Plane group symmetry was established by analysis of the images using ALLSPACE (Valpuesta et al., 1994) with IQ 1–5 up to 8 Å (Table 2, IQ = 7 × [(intensity of noise)/(intensity of signal)]). Projection maps were scaled to a maximum density of 250 and contoured in steps of 0.175 × rms densities with a negative temperature factor of −200 applied.

2.5. Mass spectrometric lipid analysis

To separate 2D crystals from empty membranes, the dialysate was briefly centrifuged (34*g*, 10 s), and the supernatant removed. The pelleted material was subsequently washed two times by resuspension in dialysis buffer followed by brief centrifugation. The three 2D crystal preparations (LPR 0.15) and purified BetPΔC45 were subjected to lipid extraction according to the method as described (Folch et al., 1957). The total lipid extracts were stored in chloroform at −20 °C. Prior to the analysis, total lipid extracts were diluted to a total lipid concentration of ~3 μM (estimated by the LPR) in methanol containing 2 μM methylamine. A mixture of internal standards was spiked into the samples at the following concentrations: 0.10 μM CL 14:0–14:0–14:0–14:0; 0.15 μM phosphatidic acid (PA) 17:0–17:0; 0.10 μM PG 17:0–17:0, 0.36 μM PI 17:0–17:0 and 0.1 μM diacylglycerol (DAG) 17:0–17:0. The quantitative lipid analysis was performed by multiple precursor ion scanning in negative ion mode as previously described (Ejsing et al., 2006) on a hybrid QSTAR Pulsar *i* quadrupole time-of-flight mass spectrometer (MDS Sciex, Concord, Canada) equipped with a robotic nanoflow ion source NanoMate HD System (Advion Biosciences, Inc., Ithaca, NJ). Twenty-one precursor ion spectra for structure-specific fragment ions produced by collision-induced dissociation of molecular anions of glycerophospholipids were acquired. The list of specific fragment ions was compiled from pre-computed *m/z* of head group derived fragment ions and acyl anions of all plausible fatty acid moieties having a total number of carbon atoms ranging from 10 to 20 with either 0, 1, or 2 double bonds. Automated processing of acquired spectra, identification and quantification of detected molecular lipid species was performed by Lipid Profiler software (MDS Sciex) as previously described (Ejsing et al., 2006).

3. Results

3.1. 2D crystallization of BetPΔC45

In the crystallization setups without any added lipids, the dialysate contained mostly protein aggregates and only very few small vesicles, which diffracted poorly to 15 Å. The number of protein aggregates was highly dependant on the amount of added lipids and was minimal at an LPR of 0.15 (w/w). Above an LPR of 0.18, reflections in the Fourier transformed image started to blur, indicating a loss of crystal order.

Initially, BetPΔC45 were grown from an *E. coli* lipid extract and had the form of small vesicles with a diameter of less than 0.5 μm. The size of these vesicles increased by adding bovine heart CL to the *E. coli* lipid extract. A maximal amount of large specimens was obtained by using a mixture of *E. coli* lipid extract/CL at 3:2 (w/w).

2D crystallization of BetPΔC45 resulted in formation of several different morphologies: sheets, planar-tubes and vesicles (Table 1). Using the mixture of *E. coli* lipid extract/CL, large vesicles and sheets were obtained after dialysis against 50 mM Tris–HCl, pH 7.5, 200 mM NaCl, 5% glycerol, 5% MPD, 4 mM $CaCl_2$, 3 mM NaN_3 (Fig. 1A), while thin planar-tubes with a width of 0.1–0.5 μm were grown via dialysis against a similar buffer replacing 200 mM NaCl by 500 mM LiCl (Fig. 1B). With *C. glutamicum* lipid extract, sheets were obtained from a

Table 1
Summary of crystal morphology, temperature requirement and resolution by using different lipids

	Dialysis buffer containing <300 mM LiCl, NaCl, or KCl	Resolution (Å)	Dialysis buffer containing >400 mM LiCl, or KCl	Resolution (Å)	Temperature (°C)	
					Incubation	Dialysis
E. coli lipid extract/CL (3:2)	Large sheets and vesicles up to 10 μm	8	Thin planar tubes (0.1 μm wide, 2-4 μm long)	—	4-room temperature (RT)	30–37
C. glutamicum lipid extract	Large sheets up to 5 μm	8	Planar tubes (0.8 μm wide,3 μm long)	9–12	RT	30
PG 16:0–18:1	Large round vesicles up to 3 μm	10–12	Not tested	—	4-RT	25–30

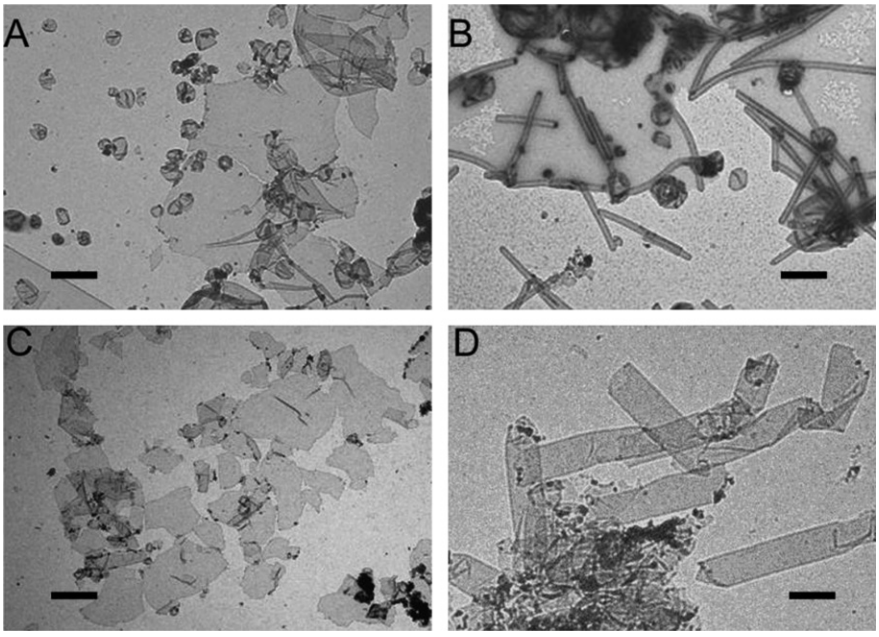

Fig. 1. Crystal morphology of BetPΔC45. The crystals were negatively stained with 1% uranyl acetate. The scale bars in each subfigure represent 1 μm. (A) Sheets and vesicles grown in the mixture of *E. coli* lipid extract/CL (3:2); (B) planar-tubes produced using the mixture of *E. coli* lipid extract/CL (3:2); (C) sheets crystals grown in the *C. glutamicum* lipid extract; (D) planar-tubes obtained by using the *C. glutamicum* lipid extract. Dialysis was performed at 37 °C for (A) and (B), and at 30 °C for (C) and (D). The dialysis buffer for (A) and (C) contained 50 mM, pH 7.5, Tris–HCl, 200 mM NaCl, 5% glycerol, 5% MPD, 4 mM $CaCl_2$, and 3 mM NaN_3. The dialysis buffer for (B) and (D) consisted of 50 mM, pH 7.5, Tris–HCl, 500 mM LiCl, 5% glycerol, 5% MPD, 4 mM $CaCl_2$, and 3 mM NaN_3.

similar buffer containing 100–300 mM LiCl, KCl, or NaCl (Fig. 1C). Planar-tubes were formed only from the dialysis buffer containing ~500 mM KCl or LiCl. These tubes could grow up to ~3 μm long and 0.8 μm wide (Fig. 1D). An intermediate concentration between 300 and 500 mM LiCl or KCl gave a mixture of sheets and planar-tubes. Negatively stained planar-tubes showed better diffraction than sheets. In contrast to LiCl and KCl, high concentration of NaCl however does not facilitate tubularization of BetPΔC45 in *C. glutamicum* lipids or in *E. coli* lipid extract/CL. Crystallization of BetPΔC45 with synthetic PG 16:0–18:1 was set up by dialysis against a buffer containing 200 mM NaCl, yielding 2D crystals in the shape of large vesicles to ~2 μm in diameter (data not shown). Several other parameters were also examined during crystallization. Temperature was found to be critical for crystallization of BetPΔC45 with *C. glutamicum* lipid extract. Before dialysis, the mixture of lipids, proteins and detergents was incubated at room temperature (Table 1). An incubation temperature less than 15 °C would lead to protein aggregation during dialysis. Dialysis temperature was restricted to 30 °C to allow a successful crystallization, while 25 °C and 37 °C led to protein aggregation (data not shown). With *E. coli* lipid extract/CL and synthetic PG 16:0–18:1, incubation temperature did not play a crucial role in crystal formation. Dialysis temperature was however spanned to a wider range of 30–37 °C for using the mixture of *E. coli* lipid extract/CL, and of 25–30 °C for PG 16:0–18:1 (Table 1). Several divalent salts in the dialysis buffer were tested ($CaCl_2$, $MgCl_2$, $CoCl_2$, $CuCl_2$, or Cd(acetate)$_2$) at concentrations of 1–10 mM. The presence of $CaCl_2$ and $MgCl_2$ as well as glycerol and MPD enlarged the size of crystalline area resulting in stronger reflections

in the Fourier transformed image, while $CoCl_2$, $CuCl_2$, and Cd(acetate)$_2$) led to protein aggregation.

3.2. Molecular packing of BetPΔC45 in 2D crystals

Sheets and vesicles grown with the mixture of *E. coli* lipid extract/CL and with the *C. glutamicum* lipid extract showed a resolution of 8 Å after image processing (Fig. 2B and F and Table 1). Vesicles formed with synthetic PG 16:0–18:1 showed weaker diffraction and rendered a resolution of 10–12 Å (Fig. 2H and Table 1). Planar-tubes in *C. glutamicum* lipid extract exhibited a resolution of 9–12 Å (Table 1, data not shown). These crystals all had rectangular unit cell dimensions with similar sizes containing two BetPΔC45 trimers (Fig. 2A, E, and G).

Crystals grown with the mixture of *E. coli* lipid extract/CL contained two BetPΔC45 trimers in a unit cell with cell dimensions 90.3×152.0 Å (Fig. 2A). A mirror-symmetric plane (the *XZ* plane) was recognized in the trimer density. Several possible plane symmetries were suggested by the program ALLSPACE: p2, p12_a, p12$_1$_b, and p222$_1$_a (Table 2). Two related trimers fitting in one unit cell can be described by either p2 or p12$_1$_b, while p222$_1$_a was suitable for four asymmetric units, and p12_a described two stacking membranes but not the relation between the two adjacent trimers in the crystal plane. This mirror symmetry as well as so many possible plane symmetries suggests that image processing led to averaging the densities of two trimers facing to different sides of the membrane: one up and one down. Different expanded unit cells in either or both directions were applied to deconvolute the averaged density. After processing, no additional data was found, the mirror symmetry remained in the projection structures (data not shown), and the symmetry was still not clear (Table 2). Therefore, it can only be explained by three reasons: (i) two stacking membranes (Fig. 2C), (ii) protein packing having a random orientation perpendicular to the membrane resulting in pseudo crystals (Fig. 2D), and (iii) small crystalline patches. By using freeze fracture microscopy, regularly stacked membranes were not found (data not shown). Image processing on a partitioned area of a raw scanned image did not help to identify small, individual crystalline patches either. Therefore, BetPΔC45 is concluded to form pseudo crystals in *E. coli* lipid extract/bovine CL.

Sheets and planar-tubes formed with the *C. glutamicum* lipid extract showed a similar unit cell size ($91.1 \pm 0.6 \times 153.5 \pm 1.4$ Å) containing two trimers (Fig. 2E). Mirror symmetry was not found in the projection structure. The only possible plane symmetry was p12$_1$_b (Table 2). The plane symmetry p12$_1$_b describes a combination of 180°-rotation and half-translation along *Y*-axis between these two trimers. Crystals grown with synthetic PG 16:0–18:1 also showed a similar unit cell size (91.7×152.7 Å) (Fig. 2G) and the same packing as the crystals in *C. glutamicum* lipid extract (Table 2). These crystals diffracted to lower resolution than the crystals in *C. glutamicum* lipid extract (Fig. 2H and Table 1), which allowed fewer significant comparisons of the plane symmetries. It explained why p222$_1$_a was also suggested but with a relatively high phase residual value (Table 2).

3.3. Molecular characterization of the lipid composition of BetP crystals

We used quantitative multiple precursor ion scanning analysis to delineate the molecular lipid composition of the total lipid extracts of the three BetPΔC45 crystals. For comparison we also analyzed a total lipid extract of the purified BetPΔC45 expressed in *E. coli*, which was used for preparing the three types of BetPΔC45 crystals.

Fig. 3 exemplifies the spectral profile obtained by multiple precursor ion scanning analysis of the total lipid extract of purified BetPΔC45. This technique detects individual glycerophospholipid species based on the molecular-specific release of fatty acid moieties as acyl anions upon fragmentation. For example, fragmentation (i.e. collision-induced dissociation) of PE 16:0–17:1 with *m/z* 702.5 promotes the release of the constituent 16:0 and 17:1 as acyl anions with *m/z* 255.23 and *m/z* 267.23 (Fig. 3). Similarly, other lipid species are resolved by their unique mass (*m/z*) and concomitant release of specific fatty acid fragment ions (Ejsing et al., 2006; Ekroos et al., 2002). Absolute quantification of glycerophospholipid species was readily achieved by spiking total lipid extracts with the unique lipid standards: PA 17:0–17:0, PE 17:0–17:0, PG 17:0–17:0, DAG 17:0–17:0, PI 17:0–17:0, and CL 14:0–14:0–14:0–14:0 (Ejsing et al., 2006). The result of the purified BetPΔC45 lipid extract showed that PE and PG species comprises 80 and 17 mol %, respectively, of the total lipid content (Table 3). Only minor amounts of PA and CL species were detected. The main lipid species extracted from purified BetPΔC45 were PE 16:0–17:1 (35 mol %), PE 16:0–19:1 (13 mol %), PE 14:0–16:0 (7 mol %), PG 16:0–17:1 (7 mol %), PE 17:1–18:1 (4 mol %), and PG 16:0–19:1 (4 mol%) (Table 3 and Fig. 3). Only a minor amount of the species CL 16:0–17:1–16:0–17:1 was identified and constituted 2 mol %. Surprisingly, this result shows that the composition of the lipid species associated with purified BetPΔC45 is very similar to the lipid composition of the *E. coli* expression system. In order to control the behavior of crystallization, lipid samples added for crystallization (the mixture of *E. coli* polar lipid extract/CL and the *C. glutamicum* lipid extract) and lipid extracts from the three crystal types were further measured by the same mass spectrometry approach. The lipid analysis of the *E. coli* polar lipid extract/CL (3:2) mixture showed that PE 16:0–17:1 was the predominant lipid species (27 mol %) together with PE 16:0–18:1 (11 mol %), PE 16:0–19:1 (7 mol %), and PE 17:1–18:1 (6 mol %) (Fig. 4). The additional bovine heart CL (CL 18:2–18:2–18:2–18:2) comprised 13 mol %. A very minor amount of CL 16:0–17:1–16:0–17:1 was detected and estimated to be less than 0.1 mol%, which can be neglected. The major lipid species in *C. glutamicum*

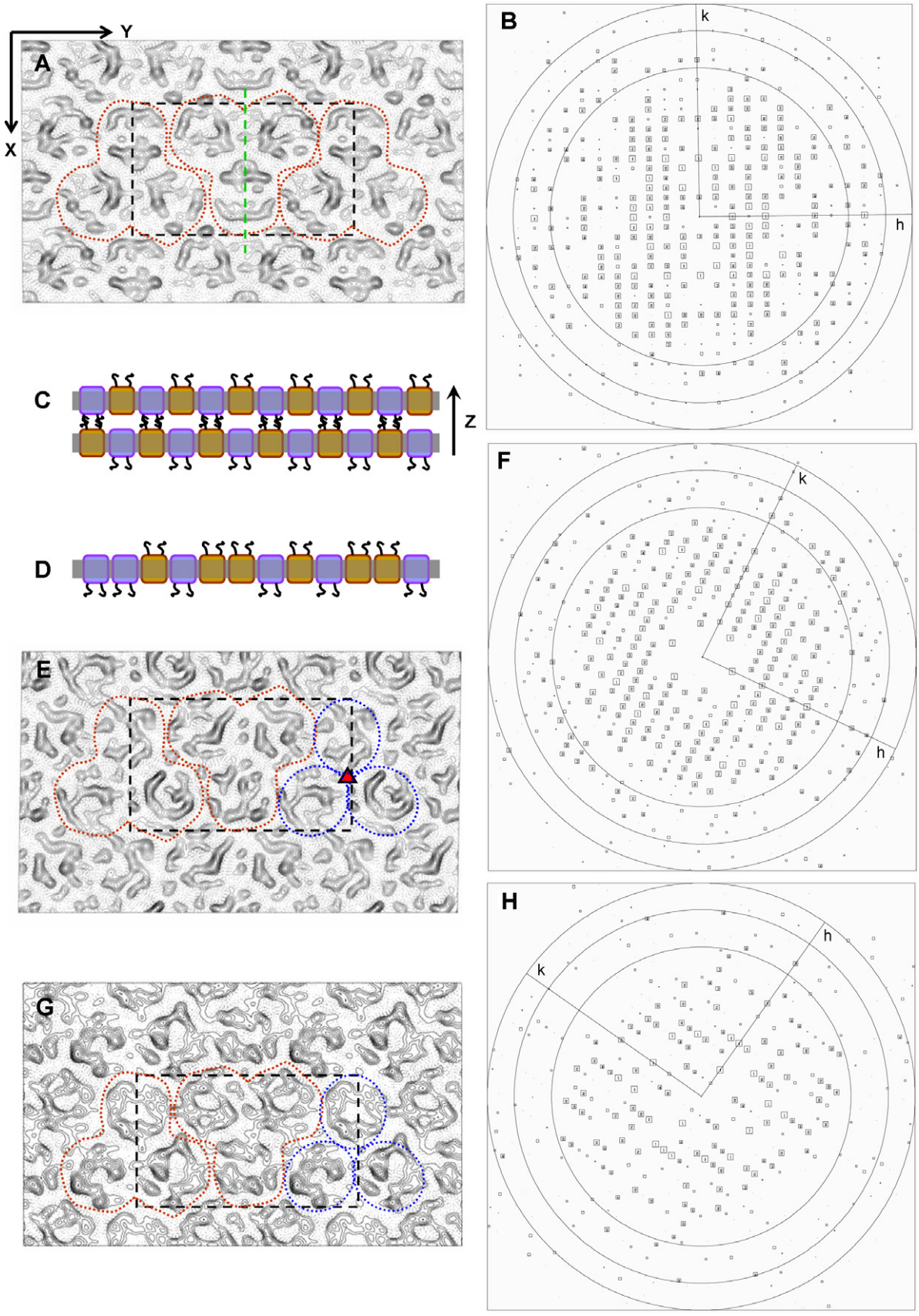
A
Y
X
B
k
h
C
Z
D
E
F
k
h
G
H
h
k

Table 2
Symmetry prediction by ALLSPACE for the crystals in three different lipids: *E. coli* lipid extract/CL (3:2, w/w), *C. glutamicum* lipid extract, and synthetic PG 16:0–18:1

Phase residue	*E. coli* lipid extract/CL sheet 90.3 × 152.0 Å	*E. coli* lipid extract/CL sheet 180.6 × 152.0 Å	*C. glutamicum* lipid extract Sheet 90.5 × 152.1 Å	*C. glutamicum* lipid extract planar-tube 91.6 × 154.8 Å	PG 16:0–18:1 vesicle 91.7 × 152.7 Å
Symmetry					
p1	25.7 (304)	28.3 (336)	28.3 (326)	25.7 (180)	28.9 (160)
p2	29.2 (152)*	35.4 (168)*	77.6 (163)	58.9 (90)	54.3 (80)
p12_b	74.3 (102)	75.2 (107)	75.5 (108)	73.8 (42)	68.0 (36)
p12_a	18.3 (103)*	18.5 (104)*	73.0 (111)	33.1 (38)[a]	36.1 (33)[a]
$p12_1$_b	19.6 (102)*	22.4 (107)*	25.7 (108)*	27.8 (42)*	31.9 (36)*
$p12_1$_a	78.6 (103)	20.0 (104)*	75.2 (111)	60.6 (38)	57.0 (33)
$p222_1$_a	23.2 (357)*	26.9 (379)*	62.5 (382)	46.0 (170)	45.4 (149)[a]
$p22_12_1$	62.5 (357)	27.5 (379)*	63.7 (382)	61.1 (170)	62.3 (149)s

Numbers in the parentheses described numbers of spots used for calculation. Reflections of IQ 1–5 to 8 Å were used for calculation.
* Acceptable suggestion based on the statistics.
[a] Possibility.

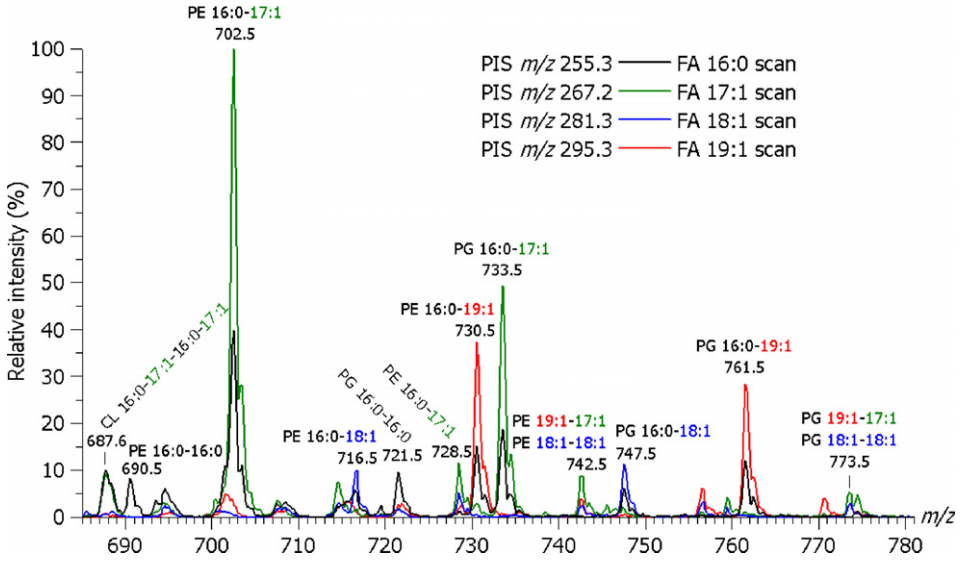

Fig. 3. Lipid profile of a total lipid extract of purified BetPΔC45 expressed in *E. coli*. The total lipid extract was analyzed by multiple precursor ion scanning analysis as described in materials and methods. The overlay of precursor ion scans for FA 16:0 (black line, PIS *m/z* 255.2), FA 17:1 (green line, PIS *m/z* 267.2), FA 18:1 (red line, PIS *m/z* 281.3), and FA 19:1 (red line, PIS *m/z* 295.3) shows detected lipid species annotated by their FA moieties. For presentation clarity, only four precursor ion spectra out of the 21 acquired are shown. The quantification of identified lipid species was achieved by spiking the total lipid extracts with known amounts of synthetic glycerophospholipid standards (one for each lipid class), having FA 17:0 moieties (for PA, PE, PG, PI and DAG) and FA 14:0 moieties (for CL) (data not shown).

lipid extract were PG 16:0–18:1 (31 mol %), CL 16:0–18:1–16:0–18:1 (26 mol %), PA 16:0–18:1 (9 mol %), PI 16:0–18:1 (6 mol %), and CL 16:0–16:0–16:0–18:1 (6 mol %) (Fig. 4). The amount of each lipid class is shown in Table 3. The lipid composition of 2D crystals formed in the presence of the mixture of *E. coli* lipid extract/CL, the *C. glutamicum* lipid extract, or synthetic PG 16:0–18:1 showed that PE species were still the major constituents of the BetP

Fig. 2. Projection maps and image Fourier transforms of sheets: (A) and (B) by using the mixture of *E. coli* lipid extract/CL (3:2); (E) and (F) by using the *C. glutamicum* lipid extract; (G) and (H) by using the synthetic PG 16:0–18:1. The projection maps were calculated to 8 Å from a single lattice, applied with the symmetry p1 and a B factor −200, scaled to a maximum density of 250, and contoured in steps of 17.5. Black dashed lines represent the unit cell size; red dashed lines mark a BetPΔC45 trimer; blue oval circles show a BetPΔC45 monomer; the green dashed line displays the mirror symmetric plane; the red triangle shows the pseudo 3-fold axis in the center of a trimer. In the image Fourier transforms, the intensity of the spots is indicated by the IQ values and the IQ values of 1–4 are displayed in the squares. IQ 1 indicates the intensity more than seven times the background and IQ 7 indicates an equal strength to the noise. The circles are drawn at 7, 8, and 10 Å resolution. (C and D) Two possible reasons for the mirror symmetric plane in the projection map (A): (C) for two stacking crystal membranes that two protein molecules; (D) for BetPΔC45 forming pseudo crystals that are well-ordered in *XY* plane but not in the direction perpendicular to the membrane plane.

Table 3
Lipid class composition of purified BetPΔC45, lipids samples, and BetPΔC45 crystals

Samples	DAG (mol %)	PA (mol %)	Cardiolipin (mol %)	PE (mol %)	PG (mol %)	PI (mol %)
Purified protein	Nil	1.0 ± 0.2	2.3 ± 0.4	79.6 ± 0.5	17.1 ± 0.5	Nil
E. coli lipid extract/CL (3:2)	Nil	0.2 ± 0.1	13.8 ± 0.5	70.7 ± 0.9	15.2 ± 0.4	Nil
C. glutamicum extract	4.5 ± 0.3	12.9 ± 0.4	32.8 ± 1.5	Nil	43.8 ± 0.6	6.0 ± 0.2
Crystals in *E. coli* lipid extract/CL (3:2)	5.6 ± 0.4	3.3 ± 0.3	4.2 ± 0.1	65.6 ± 1.1	21.3 ± 0.4	Nil
Crystals in *C. glutamicum* extract	8.5 ± 2.5	3.5 ± 0.9	9.3 ± 1.3	43.0 ± 2.8	35.7 ± 1.5	Nil
Crystals in PG 16:0–18:1	2.0 ± 0.3	0.14 ± 0.07	0.94 ± 0.08	51.7 ± 3.5	45.2 ± 3.4	Nil

Quantities of diacylglycerol (DAG), phosphatidic acid (PA), cardiolipin, phosphatidyl ethanolamine (PE), phosphatidyl glycerol (PG), and phosphatidyl inositol (PI) are compared in mol % (± standard deviation).

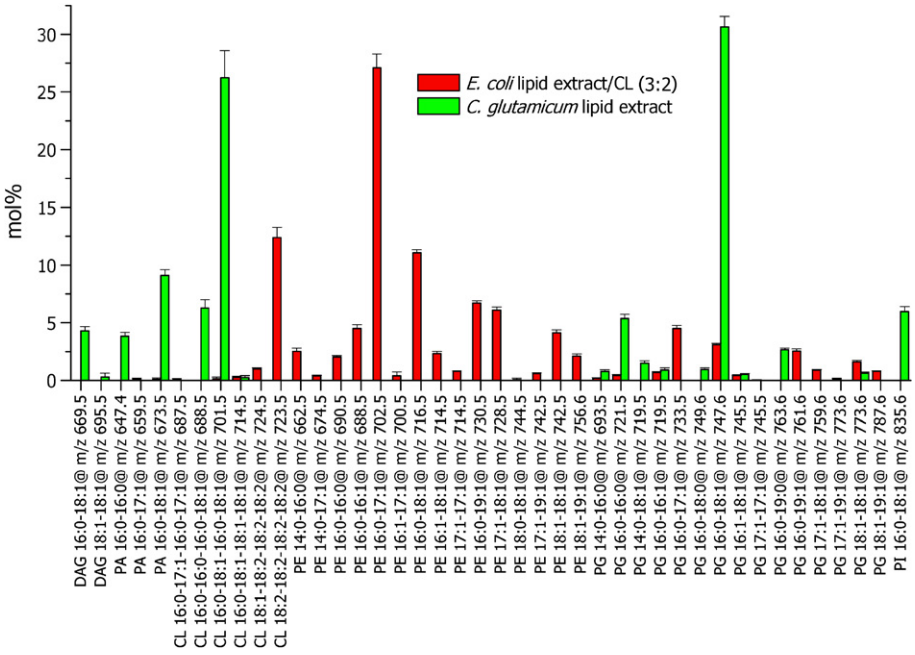

Fig. 4. Quantification of identified individual lipid species and spectral profiles obtained by lipid class-specific PIS and lipid species-specific MPIS on the mixture of *E. coli* polar lipid extract and bovine cardiolipin (3:2, w/w) and the *C. glutamicum* lipid extract used for 2D crystallization. Precursor ion spectra (PIS) at *m/z* 702.50 and 732.90 were identified as PE 16:0–17:1 and CL 18:2–18:2–18:2–18:2 for the mixture of *E. coli* lipid extract/CL. The first two dominant peaks (PIS *m/z* at 701.50 and 747.50) were identified as CL 16:0–18:1–16:0–18:1 and PG 16:0–18:1 for the *C. glutamicum* lipid extract.

crystals with 65, 43, and 52 mol %, respectively (Table 3). Other detected lipid species were PG (21%, 36%, and 45%), CL (4%, 9%, and 1%), and PA (3%, 4%, and <1%). Fig. 5 shows the amounts of the major lipid species detected in the various BetP crystals and in the purified protein. The main species detected were PG 16:0–18:1, PE 16:0–17:1, PE 16:0–19:1 and CL 16:0–18:1–16:0–18:1. Bovine CL (18:2–18:2–18:2–18:2) was surprisingly not found in the crystals formed in *E. coli* lipids/bovine CL.

4. Discussion

Based on previous studies, the osmo- and chill-sensitivity of BetP depends on the lipid composition in the membrane. Our crystallographic results also reflect that lipids influence the crystallinity of BetPΔC45. During crystallization of BetPΔC45 by using three different lipid preparations independently, the lipids specifically affect the molecular packing of proteins. BetPΔC45 crystallized with the mixture of *E. coli* lipid extract/bovine CL (3:2) formed pseudo crystals. Since PG 16:0–18:1 was the most abundant lipid species in *C. glutamicum* membranes, synthetic PG 16:0–18:1 was introduced to 2D crystallization, leading to non-pseudo crystal formation. The crystals obtained by using the *C. glutamicum* lipid extract showed the greatest advantages for structure determination in terms of the crystal packing ($p12_1\_b$) and crystal size (~5 μm). To probe the cause of different crystallinities by using different lipid preparations, we correlate crystallographic data together with MS data to monitor the lipid composition during crystallogenesis. In addition, several parameters of crystallization were found to be important to form crystals of BetPΔC45 and to induce tubularization.

4.1. Tubularization

Tubularization of 2D crystals is a complicated process. Tubularization of BetPΔC45 2D crystals could be induced

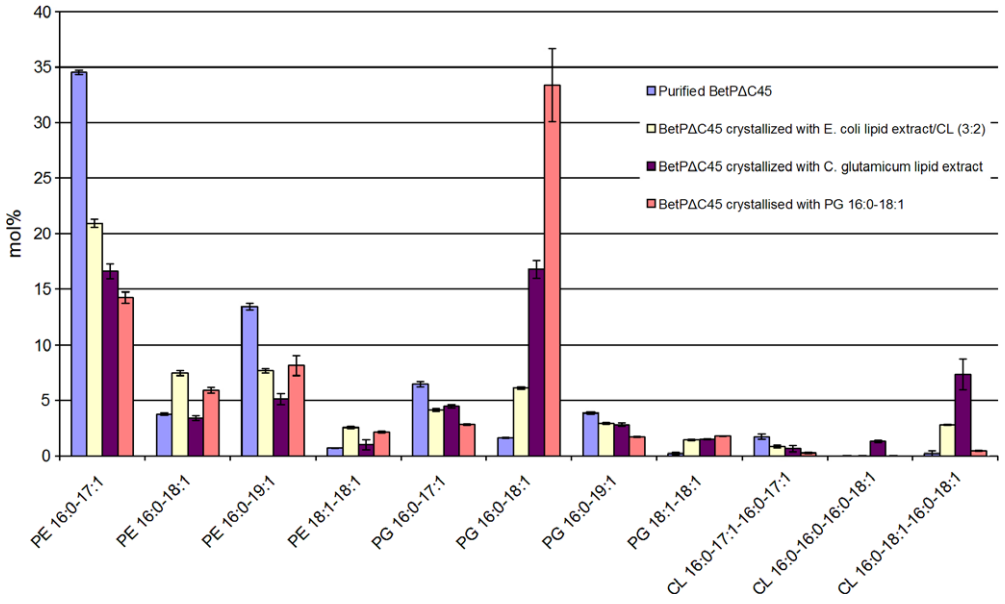

Fig. 5. Comparison of the major PE, PG and CL species detected in the total lipid extracts of purified BetPΔC45 expressed in *E. coli*, 2D crystals using the mixture of *E. coli* lipid extract/CL (3:2), synthetic PG 16:0–18:1, and the *C. glutamicum* lipid extract.

by increasing the concentration of LiCl or KCl during dialysis. Increase of NaCl concentration, however, does not facilitate tubularization of BetPΔC45, even though LiCl, NaCl, and KCl have very similar chemical properties. Several other proteins also show tubularization by increasing the salinity during dialysis (Heymann et al., 2003; Mosser, 2001). A possible explanation is that high salinity alters the water activity, which accordingly changes the potential of membrane crystals. In addition, the width of planar-tubes is influenced by lipids as well. It could be influenced by the curvature of bilayers, which was determined by the head groups and/or from the acyl moieties.

Planar-tubes formed with *C. glutamicum* lipids showed a slightly lower resolution than sheets. These two morphologies had the same unit cell dimensions and protein–protein contacts. The resolution reduced in the planar-tubes could be due to anisotropicity of "bent" crystal lattices, while sheets are evener. A similar situation was observed in OxlT, that sheets diffract to 3.4 Å while planar-tubes only reach a resolution of 6 Å. However, the sheets have a tighter packing than the planar-tubes, even though these two morphologies have the same symmetry $p22_12_1$ (Heymann et al., 2003).

4.2. Role of lipids in BetP crystallization

Escherichia coli lipids (75% PE and 19% PG) (Morein et al., 1996) and the lipids co-purified with BetPΔC45 (80% PE and 17% PG) showed nearly the same composition. It reflects that BetPΔC45 does not associate specifically with the lipids from its host organism in order to mimic the PG-rich environment of its original organism. It could be due to the detergent-rich condition during protein purification, which could weaken the specificity of proteins on lipids.

Four dominant PE and PG species with an amount of $\geqslant 5$ mol % were highlighted before and after crystallization of BetPΔC45 in the three crystal samples: PE 16:0–17:1, PE 16:0–19:1, PG 16:0–17:1, and PG 16:0–18:1. Compared to purified BetP protein, lipid extracts from all three crystals showed a decreasing amount of PE and PG with the moieties 16:0–17:1 and 16:0–19:1, while PG 16:0–18:1 were enriched in all crystals (Fig. 5). Since *C. glutamicum* does not synthesize PE class, the only source of PE is from the *E. coli* lipid extract and the expression system. In the crystals grown with *E. coli* lipids/CL, PG 16:0–18:1, PE 16:0–18:1 as well as CL 16:0–18:1–16:0–18:1 were enriched compared to the purified protein. It implies that the moieties 16:0–18:1 was enriched during crystallization.

Compared to the crystals in *E. coli* lipids/CL, those non-pseudo crystals grown with *C. glutamicum* lipids and with PG 16:0–18:1 contained a relatively high amount of PG 16:0–18:1 (17% and 33%, respectively). It is attributed that a certain amount of PG 16:0–18:1 is essential to form non-pseudo crystals. The crystals grown with synthetic PG 16:0–18:1 were found to have the highest amount of PG 16:0–18:1 but the lowest resolution (12 Å). It is possible that the order of crystals may be influenced by the double bond position in the 18:1 fatty acid chain and/or a lack of other lipid species in *C. glutamicum*. Double bonds in *cis*-configuration exhibit a kink that can alter lipid–protein interaction and bilayer curvature. It is most likely that there is a certain natural diversity in double bond position in *C. glutamicum* lipids resulting in different positions than that of synthetic PG 16:0.18:1. Besides, more CL 16:0–18:1–16:0–18:1 was found in the crystals which diffract to 8 Å (grown with *C. glutamicum* lipids and with *E. coli* lipids/CL) than the crystals in PG 16:0–18:1. It implies that CL 16:0–18:1–16:0–18:1 improves the crystal order and leads to a better resolution.

Surprisingly, no CL 18:2–18:2–18:2–18:2 was detected in the 2D crystals grown with *E. coli* lipids/bovine CL, even though an excess amount of this bovine CL was added. It shows not only that CL 18:2–18:2–18:2–18:2 is not associated with BetP, but also that this lipid is not preserved in the dialysate. The lipid extracts from crystals were prepared by organically extracting the dialysate without separating the crystals from the aggregates and empty vesicles. Since bovine CL was not detected in the crystals, it suggests that the lipids detected were from crystal membranes.

4.3. Role of CL in osmoadaption

The total amount of negatively charged lipids (PI, PG, and CL) in *C. glutamicum* membranes was about 83 mol %, and a very high amount of 32 mol % of CL was measured. In previous report, the *C. glutamicum* membrane contained 87 mol % PG and only 5 mol % of CL (Hoischen and Krämer, 1990). The difference could be explained either by using different experimental methods or by using the mutant *C. glutamicum* strain Cgl*ΔotsAΔtreSΔtreY* which misses the peptidoglycan layer of the cell wall (Wolf et al., 2003). This strain is more sensitive to growth stress, which could potentially be the reason for an enhanced CL synthesis (Özcan et al., 2007). A similar effect was observed in *Rhodobacter sphaeroides,* which responds to osmotic stress by increasing the amount of CL in the membranes (Catucci et al., 2004).

4.4. Chill activation in 2D crystallization

The influence of *C. glutamicum* lipids within the crystals can be deduced from the importance of temperature during 2D crystallization. If the proteins and *C. glutamicum* lipids were incubated beliw 15 °C, only aggregates were obtained after detergent removal. Proteins and lipids had to be incubated at about 22 °C in order to form well-ordered 2D crystals. In contrast, incubation at temperatures between 4 and 25 °C with *E. coli* lipids/CL did not affect 2D crystal formation. It is our experience that incubation of BetP and lipids before detergent removal is very important to obtain an equilibrated ternary protein–lipid–detergent system in order to prevent an immediate aggregation. Although the importance of the dialysis temperature has been reported for several other 2D crystallizations (Engel et al., 1992; Hasler et al., 1998; Heymann et al., 2003; Schmidt-Krey et al., 2007; Zhuang et al., 1999), incubation temperature is rarely mentioned. Besides, the incubation temperature was only restricted when using the natural lipids of *C. glutamicum*, which could be evidence for a specific interaction between BetP and the lipids. In previoud reports, BetP expressed in *C. glutamicum* cells is activated to transport glycine–betaine below 15 °C even without any external osmotic stress. In contrast, chill activation does not occur when BetP is expressed in *E. coli* cells (Morbach and Krämer, 2005; Özcan et al., 2005) as well as no effect of incubation temperature was observed in using the mixture of *E. coli* lipid extract/CL or pure PG 16:0–18:1. These temperature requirements of incubation respond to the chill activation observed in vivo.

4.5. Functional lipids for crystallization

Many membrane proteins have been reported to be successfully crystallized without using the lipids from the original organism. However, none of these proteins have been reported to perform a functionally related lipid–protein interaction. The question does arise: is it necessary to use the lipids from the original organism for crystallization if the lipid–protein interaction is related to the function of the protein?

The reported membrane protein crystals are grown mostly in synthetic PC lipids (Gonen et al., 2004; Heymann et al., 2003; Koning et al., 1999; Schmidt-Krey et al., 1998; Tate et al., 2001) or in *E. coli* polar lipids (Collinson et al., 2001; Hacksell et al., 2002; Williams et al., 1999) especially if they are originated from *E. coli*. Crystallization with PG and CL is not reported or generalized for most of the membrane proteins. However, the choice of lipids must be taken into account if lipid–protein interaction affects protein function. Is the protein function lipid-dependant, lipids from the original organism are naturally adapted to the needs of the protein. For example, the light harvesting complex (LHCII) have three PG and three digalactosyl diacyl glycerol (DGDG) bound to the protein trimer (Standfuss et al., 2005). Removal of PG lipids destabilizes the trimeric state (Nussberger et al., 1993) because they locate on the interface of two adjacent monomers. In contrast, 2D crystals of aquaporin-0 (AQP0) grown in dimyristoyl phosphatidylcholine (DMPC) show nine DMPC molecules per monomer, which locate on the tetramer–tetramer interface. AQP0 is not reported to have specific lipid–protein interactions or high-affinity lipid-binding sites (Gonen et al., 2005). These nine lipids filling the interfacial space between AQP0 tetramers do not play any functional role. The osmo- and chill-activation of BetP is lipid-dependent (Özcan et al., 2005; Peter et al., 1996; Rübenhagen et al., 2000). In addition to the biochemical data, we also observed that only an excess amount of PG 16:0–18:1 leads to non-pseudo crystallinity of BetPΔC45, and that incubation temperatures are related to the lipids use for crystallization. These two points therefore indicate that specific interactions between BetP and lipids. In 2D crystallization, *C. glutamicum* lipids help BetPΔC45 to form better crystals by enhancing a well-ordered packing (compared the *E. coli* lipids/CL) and by improving the resolution (compared to PG 16:0–18:1). Our results support that use of the lipids from the original organism advantages crystallization of the protein which is functionally related to lipids.

Acknowledgments

We are grateful to Ingeborg Schmidt-Krey (Georgia Institute of Technology, School of Biology, Atlanta) for the advice on crystallization screening, Janet Vonck (Max-Planck Institute of Biophysics, Frankfurt) for scutiny on image processing, Deryck Mills (Max-Planck Institute of Biophysics, Frankfurt) for electron microscope maintainance, Eva Duchoslav (MDS Sciex) for expert advice on Lipid Profiler software, and Christoph Thiele (Max-Planck Institute for Cell Biology and Genetics, Dresden) for providing synthetic PI 17:0/17:0. This work was supported by grants from the Deutsche Forschungsgemeinschaft A.S. (SFB-TR 13, project D1).

References

Catucci, L., Depalo, N., Lattanzio, V.M., Agostiano, A., Corcelli, A., 2004. Neosynthesis of cardiolipin in *Rhodobacter sphaeroides* under osmotic stress. Biochemistry 43, 15066–15072.

Collinson, I., Breyton, C., Duong, F., Tziatzios, C., Schubert, D., Or, E., Rapoport, T., Kühlbrandt, W., 2001. Projection structure and oligomeric properties of a bacterial core protein translocase. EMBO J. 20, 2462–2471.

Crowther, R.A., Henderson, R., Smith, J.M., 1996. MRC image processing programs. J. Struct. Biol. 116, 9–16.

Dumon-Seignovert, L., Cariot, G., Vuillard, L., 2004. The toxicity of recombinant proteins in *Escherichia coli*: a comparison of overexpression in BL21(DE3), C41(DE3), and C43(DE3). Protein Expr. Purif. 37, 203–206.

Ejsing, C.S., Duchoslav, E., Sampaio, J., Simons, K., Bonner, R., Thiele, C., Ekroos, K., Shevchenko, A., 2006. Automated identification and quantification of glycerophospholipid molecular species by multiple precursor ion scanning. Anal. Chem. 78, 6202–6214.

Ekroos, K., Chernushevich, I.V., Simons, K., Shevchenko, A., 2002. Quantitative profiling of phospholipids by multiple precursor ion scanning on a hybrid quadrupole time-of-flight mass spectrometer. Anal. Chem. 74, 941–949.

Engel, A., Hoenger, A., Hefti, A., Henn, C., Ford, R.C., Kistler, J., Zulauf, M., 1992. Assembly of 2-D membrane protein crystals: dynamics, crystal order, and fidelity of structure analysis by electron microscopy. J. Struct. Biol. 109, 219–234.

Folch, J., Lees, M., Sloane Stanley, G.H., 1957. A simple method for the isolation and purification of total lipides from animal tissues. J. Biol. Chem. 226, 497–509.

Gonen, T., Sliz, P., Kistler, J., Cheng, Y., Walz, T., 2004. Aquaporin-0 membrane junctions reveal the structure of a closed water pore. Nature 429, 193–197.

Gonen, T., Cheng, Y., Sliz, P., Hiroaki, Y., Fujiyoshi, Y., Harrison, S.C., Walz, T., 2005. Lipid–protein interactions in double-layered two-dimensional AQP0 crystals. Nature 438, 633–638.

Grigorieff, N., 1998. Three-dimensional structure of bovine NADH:ubiquinone oxidoreductase (complex I) at 22 Å in ice. J. Mol. Biol. 277, 1033–1046.

Hacksell, I., Rigaud, J.L., Purhonen, P., Pourcher, T., Hebert, H., Leblanc, G., 2002. Projection structure at 8 Å resolution of the melibiose permease, an Na–sugar co-transporter from *Escherichia coli*. EMBO J. 21, 3569–3574.

Hasler, L., Heymann, J.B., Engel, A., Kistler, J., Walz, T., 1998. 2D crystallization of membrane proteins: rationales and examples. J. Struct. Biol. 121, 162–171.

Heymann, J.A., Hirai, T., Shi, D., Subramaniam, S., 2003. Projection structure of the bacterial oxalate transporter OxlT at 3.4 Å resolution. J. Struct. Biol. 144, 320–326.

Hoischen, C., Krämer, R., 1990. Membrane alteration is necessary but not sufficient for effective glutamate secretion in *Corynebacterium glutamicum*. J. Bacteriol. 172, 3409–3416.

Hunte, C., Screpanti, E., Venturi, M., Rimon, A., Padan, E., Michel, H., 2005. Structure of a Na+/H+ antiporter and insights into mechanism of action and regulation by pH. Nature 435, 1197–1202.

Keilhauer, C., Eggeling, L., Sahm, H., 1993. Isoleucine synthesis in *Corynebacterium glutamicum*: molecular analysis of the ilvB-ilvN-ilvC operon. J. Bacteriol. 175, 5595–5603.

Koning, R.I., Keegstra, W., Oostergetel, G.T., Schuurman-Wolters, G., Robillard, G.T., Brisson, A., 1999. The 5 Å projection structure of the transmembrane domain of the mannitol transporter enzyme II. J. Mol. Biol. 287, 845–851.

Morbach, S., Krämer, R., 2005. Structure and function of the betaine uptake system BetP of *Corynebacterium glutamicum*: strategies to sense osmotic and chill stress. J. Mol. Microbiol. Biotechnol. 10, 143–153.

Morein, S., Andersson, A., Rilfors, L., Lindblom, G., 1996. Wild-type *Escherichia coli* cells regulate the membrane lipid composition in a "window" between gel and non-lamellar structures. J. Biol. Chem. 271, 6801–6809.

Mosser, G., 2001. Two-dimensional crystallogenesis of transmembrane proteins. Micron 32, 517–540.

Nussberger, S., Dorr, K., Wang, D.N., Kühlbrandt, W., 1993. Lipid–protein interactions in crystals of plant light-harvesting complex. J. Mol. Biol. 234, 347–356.

Özcan, N., Krämer, R., Morbach, S., 2005. Chill activation of compatible solute transporters in *Corynebacterium glutamicum* at the level of transport activity. J. Bacteriol. 187, 4752–4759.

Özcan, N., Ejsing, C.S., Shevchenko, A., Lipski, A., Morbach, S., Krämer, R., 2007. Osmolality, temperature and membrane lipid composition modulate the activity of betaine transporter BetP in *Corynebacterium glutamicum*. J. Bacteriol.

Palsdottir, H., Hunte, C., 2004. Lipids in membrane protein structures. Biochim. Biophys. Acta 1666, 2–18.

Peter, H., Burkovski, A., Krämer, R., 1996. Isolation, characterization, and expression of the *Corynebacterium glutamicum* betP gene, encoding the transport system for the compatible solute glycine betaine. J. Bacteriol. 178, 5229–5234.

Rübenhagen, R., Ronsch, H., Jung, H., Krämer, R., Morbach, S., 2000. Osmosensor and osmoregulator properties of the betaine carrier BetP from *Corynebacterium glutamicum* in proteoliposomes. J. Biol. Chem. 275, 735–741.

Ruprecht, J.J., Mielke, T., Vogel, R., Villa, C., Schertler, G.F., 2004. Electron crystallography reveals the structure of metarhodopsin I. EMBO J. 23, 3609–3620.

Schiller, D., Rübenhagen, R., Krämer, R., Morbach, S., 2004. The C-terminal domain of the betaine carrier BetP of *Corynebacterium glutamicum* is directly involved in sensing K+ as an osmotic stimulus. Biochemistry 43, 5583–5591.

Schiller, D., Ott, V., Krämer, R., Morbach, S., 2006. Influence of membrane composition on osmosensing by the betaine carrier BetP from *Corynebacterium glutamicum*. J. Biol. Chem. 281, 7737–7746.

Schmidt-Krey, I., Lundqvist, G., Morgenstern, R., Hebert, H., 1998. Parameters for the two-dimensional crystallization of the membrane protein microsomal glutathione transferase. J. Struct. Biol. 123, 87–96.

Schmidt-Krey, I., Haase, W., Mutucumarana, V., Stafford, D.W., Kühlbrandt, W., 2007. Two-dimensional crystallization of human vitamin K-dependent gamma-glutamyl carboxylase. J. Struct. Biol. 157, 437–442.

Smith, J.M., 1999. Ximdisp–A visualization tool to aid structure determination from electron microscope images. J. Struct. Biol. 125, 223–228.

Standfuss, J., Terwisscha van Scheltinga, A.C., Lamborghini, M., Kühlbrandt, W., 2005. Mechanisms of photoprotection and nonphotochemical quenching in pea light-harvesting complex at 2.5 Å resolution. EMBO J. 24, 919–928.

Tate, C.G., Kunji, E.R., Lebendiker, M., Schuldiner, S., 2001. The projection structure of EmrE, a proton-linked multidrug transporter from *Escherichia coli*, at 7 Å resolution. EMBO J. 20, 77–81.

Valpuesta, J.M., Carrascosa, J.L., Henderson, R., 1994. Analysis of electron microscope images and electron diffraction patterns of thin crystals of phi 29 connectors in ice. J. Mol. Biol. 240, 281–287.

Vinothkumar, K.R., Smits, S.H., Kühlbrandt, W., 2005. pH-induced structural change in a sodium/proton antiporter from *Methanococcus jannaschii*. EMBO J. 24, 2720–2729.

Wang, D.N., Kühlbrandt, W., 1991. High-resolution electron crystallography of light-harvesting chlorophyll a/b-protein complex in three different media. J. Mol. Biol. 217, 691–699.

Williams, K.A., Geldmacher-Kaufer, U., Padan, E., Schuldiner, S., Kühlbrandt, W., 1999. Projection structure of NhaA, a secondary transporter from *Escherichia coli*, at 4.0 Å resolution. EMBO J. 18, 3558–3563.

Wolf, A., Krämer, R., Morbach, S., 2003. Three pathways for trehalose metabolism in *Corynebacterium glutamicum* ATCC13032 and their significance in response to osmotic stress. Mol. Microbiol. 49, 1119–1134.

Yildiz, Ö., Vinothkumar, K.R., Goswami, P., Kühlbrandt, W., 2006. Structure of the monomeric outer-membrane porin OmpG in the open and closed conformation. EMBO J. 25, 3702–3713.

Zhuang, J., Prive, G.G., Werner, G.E., Ringler, P., Kaback, H.R., Engel, A., 1999. Two-dimensional crystallization of *Escherichia coli* lactose permease. J. Struct. Biol. 125, 63–75.

Ziegler, C., Morbach, S., Schiller, D., Krämer, R., Tziatzios, C., Schubert, D., Kühlbrandt, W., 2004. Projection structure and oligomeric state of the osmoregulated sodium/glycine betaine symporter BetP of *Corynebacterium glutamicum*. J. Mol. Biol. 337, 1137–1147.